RSC Advances

ROYAL SOCIETY OF CHEMISTRY

www.rsc.org/advances

Structural and electronic properties of Pd-decorated graphene oxides and their effects on the adsorption of nitrogen oxides: insights from density functional calculations

Shaobin Tang* and Jiayi Zhu

Key Laboratory of Organo-Pharmaceutical Chemistry of Jiangxi Province, Gannan Normal University, Ganzhou 341000, China

Abstract

The structural and electronic properties of Pd-decorated reduced graphene oxides (rGOs) and its effects on the adsorption of nitrogen oxides NO_x (x=1,2,3) were studied by the density functional theory calculations. Our results indicate that the Pd atom and Pd_4 and Pd_6 clusters can be strongly bound to the rGOs surface through the Pd···O coordination bond or Pd–O covalent bond between Pd and the active sites provided by the hydroxyl and epoxy functional groups. Generally, the Pd clusters exhibit more stronger binding to rGO than single metal atom. The strong binding Pd clusters to substrate effectively modifies the position of d-band center accompanied by larger charge transfer from cluster to support. The decorated Pd on rGO improves the adsorption of NO_x with larger binding energy, compared to the pristine graphene and rGO nanomaterials. The adsorption strength of gas molecule is well correlated with the d-band center of Pd cluster. The electronic structure calculations show that the strong hybridization of the frontier orbitals of free NO_2 and NO_3 with the d electronic states of decorated Pd around the Fermi level is responsible for the large charge transfers from molecules to Pd-GO complex, giving rise to the acceptor doping by these molecule on this complex, whereas the adsorbed NO shows both donor and acceptor doping character, depending on the adsorption sites of NO.

* Corresponding author. Fax: +86–797–8393536.

E-mail address: tsb1980@xmu.edu.cn

1. Introduction

Graphene, a single layer of carbon atoms formed in honeycomb lattice, has stimulated extensive research activities because of its novel electronic, optical, and mechanical properties.[1-6] Controlling the type and the density of charge carriers by doping is very important for the application of sp^2 carbon-based electronics. Owing to the high electron mobility and large specific surface area, the interactions of external molecular species with graphene, such as NO_2 and NH_3, may change the local carrier concentration and result in remarkable fluctuation of conductivity, and thus provides the promising applications in design of chemical detectors.[7-10] However, the lack of chemically active defect sites on pristine graphene results in the weak adsorption of molecular and atom species, which limits its wide use in practical sensing applications. Covalent functionalization of graphene with foreign atom or small molecular groups may provide the active sites for improving the interaction of gas molecule.

Graphene oxides (GO), a derivative of graphene, have emerged as a new class of carbon-based nanoscale materials.[11-13] By removal of oxygen groups on GO, recovery of sp^2 carbon network can be realized, and thus the chemical reduced graphene oxides (rGO) can present the high electrical conductivity. However, some oxygen groups still remain even at large reducation level.[14] These residual oxygen-containing groups on rGO may provide the active defective sites, enhancing the interaction of molecules with graphene. The recently experimental studies [15-19] reveal that the rGOs or chemically converted graphene can be served as high-performance molecular sensors, such as NO_2 , NH_3, and Cl_2. It is reported that the electron transfer from the rGO to

adsorbed molecules may be responsible for the high sensitivity, which enhanced the electrical conduction of rGO sheet. Using the density functional theory calculations, our recent studies[20,21] show that the rGOs provide many active sites, which consist of the oxygen groups and its neighboring carbon atoms for adsorption of gas molecules, increasing the binding energies and enhancing charge transfers from molecules to materials, consistent with experimental observations.[15-17]

Graphene-nanocrystals (NCs) hybrid nanostructures have attracted wide attention in energy storage/conversion devices and sensing divices due to the novel physical and chemical properties.[22] The rGO may be used as a well support of NCs or metal atoms because the oxygen-containing groups can strongly anchor NCs to the material surface. Many experimental works[23-25] show that the noble metal NCs and metal oxides, such as Ag, Pd, and SnO_2, are used to decorate the low-dimensional carbon nanomaterials for gas sensing enhancement. Recently, Li et al.[26] used the Pd-decorated rGO to fabricate the NO sensor devices, which show the high sensitivity. Based on the density functional theory calculations, Wang et al.[27] and Chen et al.[28] show that Mg and Ti atoms-doped rGO can improve the hydrogen storage capacity. It is proposed that the metal atoms could be strongly bound to the oxygen sites, preventing the metal atom from clustering. However, the metal-rGO (GO) hybrid structures are complex because of various binding mechanisms. For example, in the case of rGO, the types of oxygen functional group and arrangement of these groups as well as the oxygen level may present different influence on the interaction of NCs with surface.

Despite these important contributions, the detailed structural properties of metal-decorated rGO nanomaterials are less known, and an atomic-scale understanding on adsorption of nitrogen oxides on metal-rGO hybrid is highly required for gas sensing device. In this paper, using the density-functional theory calculations, we investigate the structural properties of palladium atom-decorated rGOs. The mechanisms for the interaction of nitrogen oxides NO_x (x=1,2,3) with Pd-rGO hybrid structure and the adsorption doping effect on their electronic properties were explored.

2. Computational details

All the calculations were performed by the density functional theory (DFT) calculations using the DMol3 package.[29] The generalized gradient approximation (GGA) in the PW91 [30]form is employed to describe the exchange-correction potential. The double numerical plus polarization function (DNP) basis set and a real-space cutoff of 5.0 Å were used. The DFT Semi-core Pseudopots (DSPP) were used for the core treatment of Pd atom. The periodic boundary supercells of 4×4 hexagonal graphene unit cells and 2×5 (or 2×6) rectangular graphene unit cells containing 40 (48) carbon atoms were used to simulate the rGO surface with low and high oxidation level, respectively. A vacuum region of 12 Å was considered to separate the layer and its images in the direction perpendicular to graphene layers. The 2D Brillouin zone was sampled by 7×7×1 *k*-points for 4×4 supercell and by 5×3×1 *k*-points for 2×5 and 2×6 supercell within the Monkhorst-Pack scheme.[31] During geometry optimization, the whole configuration was allowed to relax until all of the force components on any

atom were less than 10^{-3} au. The total energy was converged to 10^{-5} au with spin-polarized calculation. 17×17×1 *k*-points chosen according to the Monkhorst—Pack method along the periodic direction were used to acquire the electronic structures. The linear/quadratic synchronous transit (LST/QST) [32] methods was used to estimate the transition-state (TS) barriers. The charge transfer from molecule to Pd-decorated GO complex was calculated based on the Mulliken population analyses.

Many experimental and theoretical works[11-13, 33-46] have investigated the structural features of GO. It is commonly accepted that the hydroxyl (OH) and epoxy (–O–) groups are the two dominant oxygen species on the graphene basal plane, although some new oxidation species, such as the carbonyl pair and epoxy pair, have also been found.[36, 37, 39, 40] Based on the theoretical calculations, various atomic configurations of GO including disordered and ordered models were proposed. It is found that the atomic structures of GO with the aggregation of epoxide and hydroxyl groups on the graphene plane are energetically more favorable than that of other structures.[38, 44, 47] However, the complete structure and chemical composition of GO still remain unclear due to different preparation condition and randomly distribution of oxygen groups. In our computational models, thus, the local atomic structures of rGO with disordered phase only containing the hydroxyl and epoxide functional groups are simulated, and only the neutral Pd-rGO complexes are considered. When several oxygen functional groups are considered, the initial structures are constructed with these groups close to each other.

Figure 1 shows the calculated models for rGOs. When two oxygen groups are adsorbed on graphene, one epoxy (hydroxyl) group can be bound to the neighbor C–C bond (carbon atom) at the same and opposite side relative to the other epoxide group, denoted as G-2O-1 and G-2O-2 as shown in Figures 1a and b (G-O-OH-2 and G-O-OH-1 in Figures 1f and e), respectively. The total energy calculations show that the structure of GO with the these oxygen groups at the same side is only 0.16 eV higher in energy than that the opposite side for two epoxy groups (0.27 eV for both epoxy and hydroxyl groups), which are in agreement with previous results. [44, 48]

When the effect of two hydroxyl group on the interaction of Pd atom with GO is considered, two adsorption models of these hydroxyl groups are constructed, 1,4-hydroxyl group pair (see Figure 1c) and 1,2-hydroxyl group pair (Figure 1d),[38, 44] defined as G-2OH-1 and G-2OH-2, respectively. Although the GO structure with the 1,2-hydroxyl group pair is energetically the most favorable one for all adsorptions of two OH groups on graphene surface, the G-2OH-1 may be stable due to the formation of hydrogen bonds. In the case of G-2O-1 (Figure 1a) and G-2O-2 (Figure 1b), we also investigate the effect of other hydroxyl group on the Pd adsorption on GO. As shown in Figures 1g and h, the atomic arrangement of OH and epoxy groups at the opposite side relative to another epoxide (defined as G-2O-OH-2) is energetically more favorable than that of GO with the OH group at the opposite side with respect to two epoxy groups (G-2O-OH-1) by 0.51 eV.

To evaluate the binding strength between Pd and rGOs and the adsorption of nitrogen oxides on Pd-decorated rGO, the binding energies (E_b) are calculated by

$$E_b = [E(Pd) + E(GO)] - E(Pd - GO) \quad (1)$$

$$E_b = [E(g) + E(Pd - GO)] - E(g - Pd - GO) \quad (2)$$

respectively, where $E(GO)$, $E(Pd)$, $E(Pd-GO)$, $E(g)$, and $E(g-Pd-GO)$ are the total energies of isolated GO, free Pd atom (or Pd cluster), Pd-decorated GO complexs, gas molecule ***g*,** and gas molecule adsorbed on complexs, respectively. The gas molecules ***g*** represent nitrogen oxides NO_x (x=1,2,3). Note that the positive binding energies correspond to exothermicity for the interaction of metal or gas molecule with GO-based materials. The DFT implementation in DMOL3 may be prone to significant Basis Set Superposition Error (BSSE). Using the counterpoise correction suggested by Boys and Bernaedi,[49] we employed relaxed structure to estimate the BSSE corrected binding energies for selected systems. The calculations show that the BSSE correction to binding energy has less influence on the predicted tendency for interaction of Pd with rGOs.

3. Results and discussion

3.1 Interaction of Pd with rGO only containing the epoxy group

We first investigate the structural properties of Pd-decorated GO. For comparison, the adsorption of Pd atom on pristine graphene is calculated. Compared to the top and hollow sites of graphene, the Pd atom is energetically preferable to be adsorbed at the bridge site (Figure 2a) with the binding energy of 0.97 eV. When the local structure of rGO surface contains one epoxy group, the Pd atom interacts with the oxygen group through the epoxide ring opening, leading to formation of the covalent Pd–O and Pd–C bonds (Figure 2c), denoted as Pd@G-O-b. This interaction is exothermic by

1.33 eV (see Table 1), larger than adsorption of Pd on pristine graphene. Such epoxide ring opening by metal atom is consistent with previous DFT studies.[27,28] The formation of covalent Pd–O bond between Pd and epoxy group is energetically more favorable than the Pd···O coordination bond by 0.23 eV (Pd@G-O-a shown in Figure 2b). The transition-state search shows that the transformation of the coordination Pd···O to covalent Pd–O bond is kinetically facile with only energy barrier of 0.17 eV.

The presence of another epoxy group neighboring the existing epoxide may impact on the interaction of Pd with GO. Figures 2d-h and Table 1 show the optimized structures and calculated results for adsorption of Pd on G-2O-1. Owing to the adsorption of the second oxygen group, the binding of Pd to bridge site neighboring two epoxy groups of G-2O-1 (Figure 2d) is slightly stronger than that of pristine graphene with binding energy of 1.1 eV. When one (two) epoxy rings on G-2O-1 are opened by the Pd atom leading to one (two) covalent Pd–O bonds, two structural models are considered as shown in Figures 2e and h (Figures 2f and g). The total energy calculations show that the metal atom could be more strongly bound to two epoxy groups of GO surface than to one oxygen group.

As shown in Table 1, in the case of two epoxy rings opening by the Pd atom, the formation of 1,4 C–O bond pair connecting metal atom, defined as Pd@G-2O-1c shown (see Figure 2f), is energetically more favorable than that of 1,3 C–O bond pair by 0.9 eV (see Figure 2g). Such interaction mechanism of Pd is similar to our previous results for dissociation of NH_3 on GO.[21] The energy barrier for the formation of 1,4 C–O bond pair is predicted to be 0.3 eV relative to the initial state Pd@G-2O-1a (Figure 2d), suggesting the facile **r**eactivity of GO towards two epoxy

rings opening by the Pd atom.

More importantly, when another epoxy group is located at the opposite side of graphene relative to existing epoxide (Figure 1b), the interaction of Pd with rGO through the formation of Pd···O coordination bond or Pd–O covalent bond is improved, leading to binding energy of 1.27 eV for in Pd@G-2O-2a (Figure 3a) and 2.03 eV for Pd@G-2O-2b (Figure 3b), larger than the case of only one epoxy group (Table 1). The larger binding of Pd to surface may be attributed to the increased reactivity of neighboring C atom toward the Pd adsorption by the oxygen group at the opposite side.

3.2 Interaction of Pd with rGO only containing the hydroxyl group

We now focus on the interaction of Pd atom with rGO including two hydroxyl groups. Figures 3c-h and Table 2 present the geometrical structures and calculated results. Adsorption of two hydroxyl groups in the form of 1,4-OH pair at the same side of graphene (see Figure 2c) result in the significant structural distortion of local carbon network, thus, it may improve the reactivity of these carbon atoms toward Pd interaction.

The total energy calculations show that the Pd atom **e**nergetically prefers to adsorb at the hollow site of carbon ring at the opposite side relative to the nearest-neighbor 1,4-OH pair, defined as Pd@G-2OH-1b shown in Figure 3d. This adsorption leads to the binding energy of 1.52 eV, larger than the adsorption of Pd at the bridge site (Pd@G-2OH-1a in Figure 3c) and than the other adsorption structures with the formation of Pd···O coordination bond (see Figures 3e and h). Such adsorption of Pd

at the hollow site is similar with previous studies,[50] in which the metal atoms on graphene can be used as point contacts, such as Fe and Co, enhancing the adsorption of oxygen-containing groups. The formation of Pd@G-2OH-1b (Figure 3d) can be easy achieved from the initial state of Pd@G-2OH-1a (Figure 3c) because the Pd diffusion is an energy barrier-free process with an exothermicity of 0.36 eV.

Many previous works [27, 28] show that the Mg and Ti atoms can abstract the H atom of OH groups of GO to form the metal–O covalent bond. Herein, we discuss such interaction mechanism for adsorption of Pd on rGO as shown in Figures 3f and g. The total energy calculations show that the one and two H abstractions of OH by Pd atom are slightly endothermic by 0.08 eV and exothermic by 0.13 eV, respectively, suggesting that the formation of Pd–O covalent bond through the ineraction of Pd with OH group is energetically less favorable, compared to the Pd···O coordination bond between OH and the adsorbed Pd.

3.3 Interaction of Pd with rGO containing both the hydroxyl and epoxy groups

Generally, the atomic structures of GO with both epoxide and hydroxyl functional groups on the graphene basal plane are energetically more stable than that of single oxygen group. Herein, the effect of both epoxy and hydroxyl groups on adsorption of Pd on GO is discussed. Figures 4 and Table S1 present the optimized structures and calculated results. When the epoxy and hydroxyl groups in G-O-OH-1 (Figure 1e) are located at the opposite side of graphene surface each other, the interaction of Pd with one oxygen group can be improved by the other oxygen group. For example, the formation of Pd–O covalent bond of epoxy group with Pd atom

(defined as Pd@G-O-OH-1b in Figure 4b) and Pd···O coordination bond between OH and Pd (Pd@G-O-OH-1a in Figure 4a) are exothermic by 2.25 and 1.45 eV, respectively, larger than the 1.33 eV for Pd@G-O-b (Figure 2c) and 1.23 eV for Pd@G-2OH-1c (Figure 3e). In contrast, the added OH at the same side relative to epoxide has less impact on the interaction of Pd with oxygen group (Figures 4c-e).

Similarly, in the case of G-2O-1, when one OH group is added to GO surface at the opposite side relative to the epoxy group (see Figure 1g), the reactivity of neighboring epoxy groups towards the Pd adorption is increased. The optimized structure and binding energy for Pd adsorption on G-2O-OH-1 are shown in Figures 4f-i and Table S1. The interactions of Pd with G-2O-OH-1 through one or two Pd–O covalent bonds on (Figures 4g-i) are obviously more stronger than the corresponding adsorption of Pd on G-2O-1 without such OH (Figures 2d-h). This strong binding of Pd with rGO is attributed to the local structural distortion induced by the OH, improving the activity of neighboring epoxy group. For example, the formation of the Pd···O coordination bond in Pd@G-2O-OH-1a (Figure 4f) is exothermic by 1.63 eV, obviously larger than 1.27 eV for Pd@G-2O-2a (Figure 3a) and 1.1 eV for Pd@G-O-a (Figure 2b) with the same Pd···O coordination bond. The improved adsorptions of Pd are largely affected by the atomic arrangement of oxygen groups (Figure 4j).

When GO is prepared or reduced at low level, the surface of materials may include high ratio of oxygen to carbon. Herein, the effect of high oxidation level on the adsorption of Pd on GO is investigated. Our structural models of GO contain the

sp^2 carbon regions separated by sp^3 carbon strips, which are thermodynamically the most favorable based on previous results.[38,44] As shown in Figures 5a-c, the sp^3 carbon strips in rectangular graphene supercell containing 40 carbon atoms consist of one hydroxyl chain connecting two nearest-neighbor epoxy group chains (defined as GO-1). In Figures 5d-f, both the hydroxyl chain and epoxy group chains in graphene supercell with 48 carbon atoms are separated by sp^2 carbon regions each other (denoted as GO-2).

Figure 5 and Table 2 show the optimized structures and calculated results for the adsorption of Pd on GO-1 and GO-2. Comparing with rGO, the weak interaction of Pd with GO is found because the binding energies for Pd@GO-1(2)**i** (**i** = **a-c**) are obviously smaller than that of low oxidation level. The weak adsorption may be due to the reduction of the number of the delocalized π electrons and the number of the available active sites caused by the high sp^3 carbon concentration. Generally, the adsorption of Pd on GO-2 including larger sp^2 carbon regions with binding energies of 1.06-1.58 eV is much stronger than GO-1 with the values of 0.75-1.03 eV. Therefore, the rGO with low oxidation level may be more suitable for the support of metal-based nanocrystals.

3.4 Electronic properties of Pd adsorbed on rGO

To have an insight into the interaction of Pd with rGO, the spin-polarized total density of state (TDOS), the partial density of states (PDOS) of binding site O atom before and after Pd adsorption and adsorbed Pd atom, and the band structures for selected Pd-adsorbed GO systems are calculated as shown in Figure 6 and Figure S1. The

TDOS and band structure calculations show that the electronic properties of rGO are effectively tuned by the Pd insertion. The semiconducting G-2O-1 with band gap of 0.1 eV (Figure 6a) becomes metallic behavior (Figure 6c) as the Pd atom interacts with two epoxy group through 1,4-Pd–O bond pair, whereas the interaction of Pd with one epoxy group through the Pd–O and Pd–C covalent bonds increases the band gap to 0.31 eV (Figure 6d). The adsorption of Pd at the bridge site near epoxy group lead to less change in band gap of GO with 0.15 eV (Figure 6b). Similarly, the zero or small semiconducting band gaps of G-2O-2 (Figure 6g), G-2OH-2 with 0.07 eV (Figure 6e), and G-2OH-1 with 0.04 eV are increased to 0.32 eV for Pd@G-2O-2b (Figure 6h), to 0.32 eV for Pd@G-2OH-2 (Figure 6f), and to 0.14 eV for Pd@G-2OH-1**b** (Figure 6i) due to the formation the Pd–C covalent bond or Pd···O coordination bond, respectively. The increased band gaps of GO may play an important role in improving the gas molecule detection.

The interaction mechanisms of Pd with GO can be understood by the PDOS of Pd and O atoms. When the Pd atom is adsorbed at the bridge site neighboring the epoxides (see Figure 2d), the PDOS of epoxy group located at the energy level around the Fermi level (Figure S1b) is less changed in comparison to the electronic states before Pd adsorption (Figure S1a), suggesting no interaction of Pd with oxygen group. In contrast, the formations of Pd–C covalent bond and Pd···O coordination bond between Pd and epoxy or hydroxyl group lead to larger change in PDOS of Pd and oxygen group compared with isolated systems (Figures S1c-i). The strong sharp peaks close to the Fermi level for PDOS of Pd and binding site O atoms are introduced,

which are mainly contributed by the *d* orbital of Pd and *p* orbital of O. The large charge transfers of 0.13-0.46 *e* from *d* electronic states of Pd to O atom are occurred, which result in the positively charged Pd. Therefore, the orbital hybridization between Pd *d* orbital and O *p* orbital plays an important role in improving the binding of Pd with GO nanomaterials.

3.5 Adsorption of nitrogen oxides on Pd-decorated rGOs

Recently, the experiment work [26] reveals that the highly sensitive, recoverable and reliable detection of NO gas can be achieved by Pd-decorated rGO devices. Herein we investigate the interactions of nitrogen oxides with Pd atom-decorated rGO. We select Pd@G-2O-1c (Figure 2f), Pd@G-2O-1d (Figure 2g), Pd@G-2O-1e (Figure 2h), Pd@G-2OH-2 (Figure 3h), and Pd@G-O-OH-1b (Figure 4b) as the structural models of Pd-decorated GO for nitrogen oxides NO_x (x = 1-3) adsorption. In light of previous studies,[50-52] two initial configurations for the NO_2 interaction with Pd, the nitro and nitrite modes, were considered in calculation. In the nitro conformation, the NO_2 molecule is bound to the adsorbed Pd atom with the N-down orientation, whereas the oxygen atom of NO_2 is pointed to the Pd in the nitrite configuration. Similarly, two initial configurations with N and O binding sites for NO adsorption are constructed. In the case of NO_3, we only discuss the adsorption of molecule with O binding site.

Figure 7 and Table 3 display the optimized structures and calculated results for NO_2 adsorption. The calculated binding energies show that the interaction of NO_2 with Pd-decorated GO depends not only on the molecule adsorption orientation, but also on the structures of rGO. Owing to decoration of Pd on rGO surface, the predicted adsorption energies of 1.05-2.08 eV are notably larger than that of the NO_2

molecule on perfect graphene,[7] GO,[20] and single-wall carbon nanotubes (SWNTs) [50-52], suggesting a novel method for GO-based gas sensor device. The stronger adsorption of NO_2 on Pd-decorated GO may be attributed to the formation of Pd–N bond with the distance of 1.97-2.0 Å for the nitro mode and the Pd–O bond with the distance of 2-2.14 Å for the nitrite mode (Figure 7). Comparing with gas molecule adsorbed on all other Pd-decorated systems, it is found that the adsorption of NO_2 on Pd@G-O-OH-1b containing both epoxy and OH groups (Figures 7i and j) is energetically the most favorable with binding energies of 2.08 eV for the nitro configuration and 2.04 eV for the nitrite configuration.

As shown in Table 3, Charge population analyses show that the adsorptions of NO_2 gas molecule on Pd@G-2O-1c, Pd@G-2O-1d**,** and Pd@G-2O-1e for all adsorption configurations give rise to the large charge transfers of -0.22 – -0.35 *e* from gas molecule to the Pd-GO hybrid, suggesting that NO_2 behaves as an acceptor to induce hole charge carriers on nanomaterials. The NO_2-induced hole doping on GO may result in the remarkable fluctuation of conductivity, enhancing the sensor response.

Besides the inserted Pd atom, we also compare other adsorption sites for NO_2 interaction. The calculated results show that the inserted Pd atom is energetically the most favorable adsorption site compared with other sites. For example, in the case of Pd@G-2O-1c (Figure 2f), the binding of NO_2 to the carbon atom away from the Pd–O bond and to the neighboring carbon atom at the opposite side relative to the Pd–O bond is endothermic by 0.38 eV and exothermic by 0.17 eV, respectively. The

noncovalent interaction of NO_2 with Pd@G-2O-1c in the direction parallel to the graphene plane is more stronger than that of pristine graphene with binding energy of 0.71 eV.

We now discuss the adsorption of NO_3 and NO on Pd-decorated rGO surface. Figure 8 and Table 4 present the optimized structures and calculated results. The interaction of NO_3 with Pd-decorated GO, which leads to two equivalent Pd–O bonds with separation of 2.12-2.18 Å (see Figures 9a and d), is exothermic by 2.76 eV for Pd@G-2O-1c and by 3.14 eV for Pd@G-O-OH-1b, remarkably larger than NO_2 adsorption on GO-based surface. Similar to the NO_2 interaction, the NO_3 adsorption induces a relatively notable charge transfer (about -0.36 *e*) from NO_3 to Pd-GO complex (Table 5), suggesting that NO_3 behaves as a acceptor.

For the adsorption of NO, the calculated results (see Figures 8b-c and e-f and Table 4) show that interaction of NO with Pd-decorated GO is determined by the Pd-GO structures, and especially by the adsorption orientation. The NO adsorptions in N-down orientation with binding energy of 1.83 eV for Pd@G-2O-1c and 2.32 eV for Pd@G-O-OH-1b are energetically more favorable than the adsorption in O-down orientation by 1.11 and 1.36 eV, respectively. In contrast to NO_2 and NO_3 adsorption, the charge transfers of 0.01-0.05 *e* from NO to Pd-decorated GO surface (Table 5) indicate a donor character of NO regardless of the adsorption configurations, consistent with experimental observations.[26] Comparing with the previous results for NO adsorption on pristine GO[20] and graphene,[7] the decorated Pd atom improves the adsorption of NO due to the formation of Pd–N or Pd–O bond.

3.6 Electronic properties of nitrogen oxides adsorbed on Pd-rGO complex

To understand the interaction mechanism for the adsorption of gas molecule on Pd-decorated GO, we perform the calculations on the spin-polarized TDOS for selected systems, PDOS of Pd and adsorbed sites N or O atoms, and DOS of gas molecule in the adsorbed and free states (see Figure 9). The TDOS calculations show that the number of electronic states at the Fermi level for spin-up and spin-down channels of Pd@G-2O-1**c** is significantly increased by the NO_2 or NO_3 adsorption (Figures 9d, f, and k) compared with that of complex without gas molecules (Figure 6c) regardless of the adsorption orientation, suggesting the enhanced conductivity of Pd-decorated GO upon exposure to these gas molecules, whereas the metallic electronic property of Pd@G-O-OH-1b (Figure 9c) becomes as the semiconducting one after the NO_2 adsorption (Figure 9h). Based on the TDOS, it is found that the NO_2 and NO_3 adsorptions on Pd-GO complex result in the downshift of the Fermi level relative to this complex without molecule interaction, acting as a *p*-type doping.

When NO_2 and NO_3 molecules are adsorbed at Pd@G-2O-1c and Pd@G-O-OH-1b in the nitro (see Figures 7a and i) and nitrite constructions (Figures 7b and j) and at Pd@G-2O-1c (Figure 8a), respectively, the PDOS of Pd and gas molecules (Figures 9e, g, i, j, and l) are obviously changed in comparison to the free states (Figures S1c and Figures 10a-c), suggesting the strong binding of gas molecules with Pd-decorated GO materials. According to the PDOS of gas molecules and Pd, the spin-up HOMO orbitals of free NO_2 and NO_3 are still occupied after adsorption, whereas the hybridization of LUMO for spin down with the d electron states of Pd

near the Fermi level results in the fully occupied LUMO orbital. This strong orbital hybridization between Pd and adsobed gas molecules gives rise to the net large charge transfers of 0.22-0.35 and 0.36 *e* from Pd-GO complex to NO_2 and NO_3.

We carefully compare the PDOS of NO_2 adsorbed on Pd-rGO hybrid in the nitro and nitrite configurations, as shown in Figures 9e, g, i, and j, and find the large differences in PDOS between the four adsorption structures. The electrons from HOMO orbtials of NO_2 adsorbed on Pd@G-2O-1c in nitro configuration for both spin channels are in wide energy range between ~-1.2 and 0 eV below the Fermi level (Figure 9e), while these PDOS peaks for other three structures (Figures 9g, i, and j) are mainly located at about -0.2, -1.2, and -0.5 eV below the Fermi level, respectively. Further calculations show that the difference of PDOS near the Fermi level is caused by adsorption orientation. The HOMO orbtials of adsorbed NO_2 are mainly contributed by N or O atoms of NO_2, depending on the nitro (Figure 9i) and nitrite model (Figures 9g and j).

The spin-polarized DOS calculations (Figures 9d-g and 9k-l) and spin densities (Figures 10a-c) show that the NO_2 and NO_3 adsorptions induce the magnetic properties on Pd-decorated rGO materials. The magnetic moments of complex are estimated to be 0.29 μ_B for NO_2 adsorption in the nitro configuration, 0.46 μ_B for the nitrite configuration, and 0.38 μ_B for NO_3 adsorption. However, the magnetic properties of pristine Pd@G-O-OH-1b (Figure 9c) can be quenched upon the NO_2 adsorption due to the spin degeneracy of electron states (see Figures 9h-j). This results provide a novel pathway to high-temperature magnetic order in graphene-based

materials.[53]

To further understand the charge transfer mechanism between Pd-GO complex and adsorbed gas molecule, the charge density difference, $\Delta\rho = \rho(g-Pd-GO) - \rho(Pd-GO) - \rho(g)$, is calculated, where $\rho(g-Pd-GO)$, $\rho(Pd-GO)$, and $\rho(g)$ represent the total charge densities of Pd-decorated GO with gas molecule adsorption, pristine Pd-GO complex, and free gas molecule, respectively. It is clearly shown from Figures 10d-f that the NO_2 and NO_3 adsorptions on Pd@G-2O-1**c** complex induce redistribution of the charge densities with electron accumulation on the adsorbed molecule and with electron depletion on the Pd atom. The inserted Pd atoms transfer large charges to the adsobed NO_2 or NO_3 molecules, which is independent of adsoprtion orientation.

3.7 Adsorption of NO on Pd nanoclusters deposited on rGO

As discussed above, the Pd atoms are able to easily diffuse on rGO surface due to the lower diffusion energy barrier, suggesting the facile formation of clusters of nanoparticles (NPs). Present calculated results are consistent with the experimental work, [23-26] in which the metal NPs are effectively coupled with rGOs with the improved sensing performance compared with isolated NPs and rGOs. Herein, the structural and electronic properties of Pd_4 and Pd_6 nanoclusters adsorbed on rGO and are discussed. The tetrahedral and octahedral configurations are used to simulate the Pd_4 and Pd_6, respectively, and only the structure of rGO with G-2O-1 (Figure 1a) is considered for deposition of Pd clusters.

Figures 11a-d and Figure S2 show the optimized structures for adsoprtion of Pd_4

and Pd_6 on G-2O-1. Various geometry structures are obtained due to the different sites of cluster relative to the graphene plane. Similar to adsorption of isolated metal atom, one Pd atom of clusters can be bound to one (see Figures 11a and Figure S2b) or two (Figure 11c and d) epoxy groups through Pd–O covalent bond. Interestingly, the optimized structures show that Pd–Pd bond of Pd clusters is able to open the epoxy group of rGO (Figure 11b and Figure S2a), leading to oxygen species located at bridge site of cluster with separation of 2.07-2.26 Å.

From Figures 11a-d, the structures of Pd cluster almost remain the same with isolated one after interaction with rGO, although the Pd–Pd bonds neighboring the bound O and C atom are elongated. In addition, the small distances of 2.28-2.45 Å between Pd and graphene carbon network, **which lead to** the significative Pd–C bond, may play an important role in improving interaction of cluster with rGOs. The binding energies of clusters are estimated to be 2.54-2.65 eV for Pd_6 and 2.13-2.27 eV for Pd_4, suggesting strong binding of Pd systems to rGO and size-dependent interfacial interaction. The strong interaction between Pd cluster and rGO is also confirmed by the TDOS of Pd-rGO complex and PDOS of Pd before and after Pd adsorption as shown i**n Figure S3.**

The electronic and magnetic properties of Pd clusters are well tuned by interfacial interaction with rGO. As shown in Figures 11c and d, the formation of bonds between Pd atoms and oxygen of rGO decreases the magnetic moment of isolated nanoclusters from 1.9 to 1.32 μ_B and to 1.68 μ_B based on the spin density calculations (see Figure 10i), respectively. The d-band centre (ε_d) provides a good

measure of chemical reactivity of transition metal surface.[54] Comparing with the freestanding Pd clusters, it is clearly shown (Table 5) that the position of ε_d of Pd particles deposited on rGO is well tuned. All Pd atoms of the isolated Pd_6 have the same ε_d of -1.37 eV each other because of the symmetry of structure. The Pd**1** atom has the lowest ε_d (-2.23 eV) among all Pd atoms, followed by Pd**3** and Pd**5** (-1.83 eV), which are further away from the Fermi level than the isolated cluster. The formation of covalent bond of these Pd with oxygen and carbon atoms may be responsible for downshift of ε_d.

The change in ε_d of Pd atoms can be explained by the excess charge of Pd_6 system over the isolated Pd cluster and rGO. The large positive excess charges on the adsorbed Pd_6 system suggest that the electrons of 0.45 e^- from rGO are transferred to the Pd cluster, consistent with the isolated Pd atom, further demonstrating strong binding of Pd cluster on rGO. To further understand the charge transfer between Pd clusters and rGO, the charge density difference is calculated, where the yellow and blue regions indicate the areas of charge accumulation and depletion, respectively. It is obvious from Figures 10g and h that the charge densities are redistributed with electron accumulation on O atoms and with electron depletion mainly on Pdx atoms (x = **1**, **3**, **5**) of cluster after deposition. The induced large charge transfers from these bound Pd atoms to rGO (0.28 *e* for Pd**1** and 0.08 *e* for Pd**3** and Pd**5**) explain the more prominent change in ε_d than other Pd atoms.

To understand the reactive activity of particles deposited on rGO, the adsorption of NO on Pd cluster with N-down orientation is discussed. We use the models shown

in Figures 11c and d to simulate the interaction with gas molecule, defined as Pd6@ G-2O-1-a and Pd6@ G-2O-1-b, respectively, and two types of adsorption site marked by Figures 11c and d, top **1**-**6** and bridge **a**-**c** sites, are considered. Figures 11e-h and Figures S2c-f and Table 4 display the optimized structures and calculated results. The large adsorption energies of 1.84-2.06 eV for top site and 1.74-2.0 eV for bridge site reveal strong interaction between NO and Pd cluster, consistent with the experimental observations [26], in which the effective detection of NO is achieved by Pd-rGO hybrid sensor devices.

The most energetically favorable adsorption site of NO is Pd**4**, followed by Pd**2** or Pd**6** because their d-band centres are more closer to the Fermi level than other Pd atoms.[55,56] During geometry optimization, no adsorption of NO at Pd**1** is found because of the lowest ε_d of this atom. As a result, the NO is adsorbed at the adjacent bridge site **a** instead of Pd**1** (Figure 11g). However, the complex structure with NO located at Pd**5** (or Pd**3**) with the next lowest ε_d is obtained (Figure S2c) beacuse the significative bond between these Pd and graphene is broken, improving the value of ε_d. Similarly, the well correlation of binding strength of gas molecule to the ε_d may also be applied to the case of isolated Pd atom adsorbed on rGO.

The charge population calculations (Table 4) show that the adsorbed NO on Pd nanocluster supported on rGO exhibit both donor and, more unexpectedly, acceptor character, depending on adsorption sites, qualitatively different from the isolated Pd atom. The electrons of 0.035-0.04 *e* from NO for top site are transferred to Pd-rGO hybrid, suggesting donor doping character of gas molecule, whereas NO accept

0.04-0.7 *e* from this hybrid as gas molecule is adsorbed at bridge site of Pd–Pd bond. Therefore, the Pd cluster deposited on rGO provides a promising way for gas sensor device.

4. Conclusions

The first-principles calculations have been used to investigate the structural properties of Pd-decorated rGOs and its effects on the interaction of nitrogen oxides NO_x (x=1, 2, and 3) with rGOs. Our calculations reveal that the Pd atom and clusters can strongly bind to the rGOs surface due to the presence of diverse active defect sites provided by the hydroxyl and epoxy functional groups and the carbon atoms near these groups. The Pd decoration on surface effectively modifies the electronic properties of the rGO nanomaterials, and even increases the semiconducting band gap of rGO. The strong binding of Pd NPs to rGO leads to large change in the d-band centre accompanied by larger charge transfer from cluster to support.

The nitrogen oxides NO_x (x=1, 2, and 3) are strongly chemisorbed on the Pd-decorated GO with the larger binding energy, compared to pristine graphene and rGO nanomaterials. Generally, the adsorption interaction of NO_3 on Pd-GO complex is relatively stronger than other nitrogen oxides, and the NO adsorption can be comparable to that of NO_2. The strong hybridization of frontier orbitals of NO_2 and NO_3 with the d electronic states of decorated Pd atom around the Fermi level leads to the large charge transfers from molecules to Pd-GO complex, giving rise to the acceptor doping by these molecule on complex, whereas the adsorbed NO acts as the donor or acceptor doping character. Therefore, the Pd-decorated GO with various

active sites of the oxygen functional groups may provide the promising applications for design of novel chemical sensor devices.

Acknowledgements. This work was supported by the National Science Foundation of China (21103026). We acknowledge simulating discussions with Z. Cao and thank the computational resources and assistance provided by the State Key Laboratory of Physical Chemistry of Solid Surfaces (Xiamen University).

Electronic Supplementary Information (ESI) available: Optimized structures, TDOS and PDOS, and calculated results for other Pd-rGO complex structures. See DOI:10.1039/b000000x/

References

1 K. S. Novoselov, A. K. Geim, S. V. Morozov, D. Jiang, Y. Zhang, S. V. Dubonos, I. V. Grigorieva and A. A. Firsov, *Science*, 2004, **306**, 666.

2 K. S. Novoselov, A. K. Geim, S. V. Morozov, D. Jiang, M. I. Katsnelson, I. V. Grigorieva, S. V. Dubonos and A. A. Firsov, *Nature*, 2005, **438**, 197.

3 K. S. Novoselov, D. Jiang, F. Schedin, T. J. Booth, V. V. Khotkevich, S. V. Morozov and A. K. Geim, *Proc. Natl. Acad. Sci. U.S.A.*, 2005, **102**, 10451.

4 A. K. Geim and K. S. Novoselov, *Nat. Mater.*, 2007, **6,** 183.

5 A. H. Castro Neto, F. Guinea, N. M. R. Peres, K. S. Novoselov and A. K. Geim, *Rev.*

Mod. Phys. 2009, **81**, 109.

6 Y. Zhang, Y.-W. Tan, H. L. Stormer and P. Kim, *Nature*, 2005, **438**, 201.

7 O. Leenaerts, B. Partoens and F. M. Peeters, *Phys. Rev. B*, 2008, **77**, 125416.

8 F. Schedin, A. K. Geim, S. V. Morozov, E. W. Hill, P. Blake, M. I. Katsnelson and K. S. Novoselov, *Nat. Mater.*, 2007, **6**, 652.

9 T. O. Wehling, K. S. Novoselov, S. V. Morozov, E. E. Vdovin, M. I. Katsnelson, A. K. Geim, and A. I. Lichtenstein, *Nano Lett.*, 2008, **8**, 173.

10 A. Sakhaee-Pour, M. T. Ahmadian, and A. Vafai, *Solid State Commun.* 2008, **147**, 336.

11 S. Watcharotone, D. A. Dikin, S. Stankovich, R. Piner, I. Jung, G. H. B. Dommett, G. Evmenenko, S.-E. Wu, S.-F. Chen, C.-P. Liu, S. T. Nguyen and R. S. Ruoff, *Nano Lett.* 2007, **7**, 1888.

12 G. Eda, G. Fanchini and M. Chhowalla, *Nat. Nanotechnol.*, 2008, **3**, 270.

13 H. A. Becerril, J. L. Mao, Z., R. M. Stoltenberg, Z. Bao and Y. Chen, *ACS Nano*, 2008, **2**, 463.

14 S. Gilje, S. Han, M. Wang, K. L. Wang and R. B. Kaner, *Nano Lett.* 2007, **7**, 3394.

15 J. D. Fowler, M. J. Allen, V. C. Tung, Y. Yang, R. B. Kaner, and B. H. Weiller, *ACS Nano***,** 2009, **3**, 301.

16 Y. Dan, Y. Lu, N. J. Kybert, Z. Luo and A. T. C. Johnson, *Nano Lett.,* 2009, **9**, 1472.

17 J. T. Robinson, F. K. Perkins, E. S. Snow, Z. Wei and P. E. Sheehan, *Nano Lett.*, 2008, **8**, 3137.

18 F. Yavari and N. Koratkar, *J. Phys. Chem. Lett.,* 2012, **3**, 1746.

19 V. Dua, S. P. Surwade, S. Ammu, S. R. Agnihotra, S. Jain, K. E. Roberts, S. Park, R. S. Ruoff and S. K. Manohar, *Angew. Chem. Int. Ed.*, 2010, **49**, 2154.

20 S. Tang and Z. Cao, *J. Chem. Phys.*, 2011, **134**, 044710.

21 S. Tang and Z. Cao, *J. Phys. Chem. C,* 2012, **116**, 8778.

22 S. Cui, S. Mao, G. Lu and J. Chen, *J. Phys. Chem. Lett.*, 2013, **4**, 2441.

23 S. Mao, S. M. Cui, G. H. Lu, K. H. Yu, Z. H. Wen and J. H. Chen, *J. Mater. Chem.*, 2012, **22**, 11009.

24 S. M. Cui, H. H. Pu, G. H. Lu, Z. H. Wen, E. C. Mattson, C. Hirschmugl, M. Gajdardziska-Josifovska, M. Weinert and J. H. Chen, *ACS Appl. Mater. Interfaces*, 2012, **4**, 4898.

25 S. M. Cui, S. Mao, Z. H. Wen, J. B. Chang, Y. Zhang and J. H. Chen, *Analyst*, 2013, **138**, 2877.

26 W. Li, X. Geng, Y. Guo, J. Rong, Y. Gong, L. Wu, X. Zhang, P. Li, J. Xu, G. Cheng, M. Sun and L. Liu, *ACS Nano*, 2011, **5**, 6955.

27 L. Wang, K. Lee, Y.-Y. Sun, M. Lucking, Z. Chen, J. J. Zhao and S. B. Zhang, ACS Nano, 2009, **3**, 2995.

28 C. Chen, J. Zhang, B. Zhang and H. M. Duan, *J. Phys. Chem. C*, 2013, **117**, 4337.

29 B. Delley, *J. Chem. Phys.* 1990, **92**, 508.

30 J. P. Perdew and Y. Wang, *Phys. Rev. B*, 1992, **45**, 13244.

31 H. J. Monkhorst and J. D. Pack, *Phys. Rev. B*, 1976, **13**, 5188.

32 N. Govind, M. Petersen, G. Fitzgerald, D. king-Smith and Andzelm, *J. Comput. Mater. Sci.,* 2003*,* **28**, 250.

33 G. Eda, Y.-Y. Lin, S. Miller, C.-W. Chen, W.-F. Su and M. Chhowalla, *Appl. Phys.*

Lett., 2008, **92**, 233305.

34 J. Wu, H. A. Becerril, Z. Bao, Z. Liu, Y. Chen and P. Peumans, *Appl. Phys. Lett.*, 2008, **92**, 263302.

35 W. Cai, R. D. Piner, F. J. Stadermann, S. Park, M. A. Shaibat, Y. Ishii, D. Yang, A. Velamakanni, S. J. An, M. Stoller, J. An, D. Chen and R. S. Ruoff, *Science*, 2008, **321**, 1815.

36 A. Bagri, R. Grantab, N. V. Medhekar and V. B. Shenoy, *J. Phys. Chem. C*, 2010, **114**, 12053.

37 A. Bagri, C. Mattevi, M. Acik, Y. J. Chabal, M. Chhowalla and V. B. Shenoy, *Nat. Chem.*, 2010, **2**, 581.

38 J.-A. Yan, L. Xian and M. Y. Chou, *Phys. Rev. Lett.*, 2009, **103**, 086802.

39 W. Zhang, V. Carravetta, Z. Li, Y. Luo and J. Yang, *J. Chem. Phys.*, 2009, **131**, 244505.

40 Z. Li, W. Zhang, Y. Luo, J. Yang and J. G. Hou, *J. Am. Chem. Soc*, 2009, **131**, 6320.

41 A. Lerf, H. He, M. Forster and J. Klinowski, *J. Phys. Chem. B*, 1998, **102**, 4477.

42 X. Li, G. Zhang, X. Bai, X. Sun, X. Wang, E. Wang and H. Dai, *Nat. Nanotechnol.*, 2008, **3**, 538.

43 W. Gao, L. B. Alemany, L. Ci and P. M. Ajayan, *Nat. Chem.*, 2009, **1**, 403.

44 J.-A. Yan and M. Y. Chou, *Phys. Rev. B*, 2010, **82**, 125403.

45 H.-K. Jeong, Y. P. Lee, R. J. W. E. Lahaye, M.-H. Park, K. H. An, I. J. Kim, C.-W. Yang, C. Y. Park, R. S. Ruoff and Y. H. Lee, *J. Am. Chem. Soc.*, 2008, **130**, 1362.

46 K.-Y. Lian, Y.-F. Ji, X.-F. Li, M.-X. Jin, D.-J. Ding and Y. Luo, *J. Phys. Chem. C*, 2013, **117**, 6049.

47 R. Larciprete, S. Fabris, T. Sun, Paolo Lacovig, A. Baraldi and S. Lizzit, *J. Am. Chem. Soc.*, 2011, **133**, 17315.

48 R. J. W. E. Lahaye, H. K. Jeong, C. Y. Park and Y. H. Lee, *Phys. Rev. B*, 2009, **79**, 125435.

49 F. S. Boys and F. Bernardi, *Mol. Phys.* 1970, **19**, 553

50 W.-L. Yim, X. G. Gong and Z.-F. Liu, *J. Phys. Chem. B,* 2003, **107**, 9363.

51 F. Mercuri, A. Sgamellotti, L. Valentini, I. Armentano and J. M. Kenny, *J. Phys. Chem. B*, 2005, **109**, 13175.

52 S. Tang and Z. Cao, *J. Chem. Phys.*, 2009, **131**, 114706.

53 D. M. Edwards and M. I. Katsnelson, *J. Phys.: Condens. Matter*, 2006, **18**, 7209.

54 B. Hammer and J. K. Nørskov, Surf. Sci. 1995, **343**, 211.

55 D.-H. Lim, A. S. Negreira and J. Wilcox, *J. Phys. Chem. C*. 2011, **115**, 8961.

56 G. Kim, Y. Kawazoe and K.-R. Lee, *J. Phys. Chem. Lett.* 2012, **3,** 1989.

Table 1: Summary of calculated results for the adsorption of Pd on graphene and rGOs with only epoxy group: the binding energy (E_b), the distance between Pd and its nearest-neighboring C (d_1), and O (d_2) atoms.

Structure*	binding site	E_b (eV)	d_1 (Å)	d_2 (Å)
Pd@G	C	0.97	2.21	
Pd@G-O-a	C	1.1	2.12	2.7
Pd@G-O-b	C and O	1.33	2.18	2.14
Pd@G-2O-1a	C	1.1	2.19	
Pd@G-2O-1b	C and O	0.83	2.03	2.2
Pd@G-2O-1c	O	2.4		1.97
Pd@G-2O-1d	O	1.5		1.97
Pd@G-2O-1e	C and O	1.44	2.11	2.03
Pd@G-2O-2a	C and O	1.27	2.1	2.73
Pd@G-2O-2b	C and O	2.03	2.15	2.09

* The corresponding structures are shown in Figures 2 and 3a-3b.

Table 2: Summary of calculated results for the adsorption of Pd on GOs with two hydroxyl groups and with high oxidation level: the binding energy (E_b), the distance between Pd and its neighboring C (d_1), and O (d_2) atoms.

Structure*	binding site	E_b (eV)	d_1 (Å)	d_2 (Å)
Pd@G-2OH-1a	C	1.16	2.22	
Pd@G-2OH-1b	C	1.52	2.36	
Pd@G-2OH-1c	C	1.23	2.14	2.54
Pd@G-2OH-1d	O	-0.08		2
Pd@G-2OH-1e	O	0.13		1.96
Pd@G-2OH-2	C	1.32	2.1	2.46
Pd@GO-1a	C	1.03	2.23	
Pd@GO-1b	C and O	0.86	2.13	2.1
Pd@GO-1c	O	0.75		2.02 (2.36)
Pd@GO-2a	C	1.58	2.1(2.25)	
Pd@GO-2b	O	1.06		2.03 (2.26)
Pd@GO-2c	O	1.1		1.99

* The corresponding structures are shown Figures 3c-3h and 5.

Table 3: Summary of calculated results for the adsorption of NO_2 on Pd-decorated rGOs: the binding energy (E_b), the distance (d_1) between binding sites N or O from NO_2 and Pd, two N–O bond lengths of NO_2 (d_2 and d_3), and the charge transfers from the molecule to Pd-GO complex (ΔQ).

Structure*	orientation	E_b (eV)	d_1 (Å)	d_2 (Å)	d_3 (Å)	ΔQ (e)
Pd@G-2O-1c	N down	1.65	1.97	1.25	1.21	-0.22
Pd@G-2O-1c	O down 1	1.05	2	1.31	1.21	-0.25
Pd@G-2O-1c	O down 2	1.68	2.1	1.28	1.28	-0.35
Pd@G-2O-1d	N down	1.88	1.97	1.27	1.21	-0.23
Pd@G-2O-1d	O down	1.24	2	1.33	1.21	-0.28
Pd@G-2O-1e	N down	1.84	2	1.27	1.2	-0.23
Pd@G-2OH-2	O down	1.59	2.14(2.23)	1.28	1.28	-0.39
Pd@G-2OH-2	N down	1.72	1.99	1.25	1.21	-0.23
Pd@G-O-OH-1b	N down	2.08	1.99	1.26	1.22	-0.23
Pd@G-O-OH-1b	O down	2.04	2.1 (2.17)	1.27	1.29	-0.36

* The corresponding structures are shown Figure 7.

Table 4: Summary of calculated results for the adsorption of NO_3 and NO on Pd-decorated rGOs: the binding energy (E_b), the distance (d_1) between gas molecule and Pd, the N–O bond lengths of NO_3 or NO (d_2), and the charge transfers from the molecule to Pd-decorated rGO (ΔQ).

Structure*	adsorbate	adsorbed site	E_b (eV)	d_1 (Å)	d_2 (Å)	ΔQ (e)
Pd@G-2O-1c	NO_3	O	2.76	2.12	1.3(1.21)	-0.36
Pd@G-2O-1c	NO	N	1.83	1.83	1.17	0.02
Pd@G-2O-1c	NO	O	0.72	2.06	1.18	0.02
Pd@G-O-OH-1b	NO_3	O	3.14	2.18	1.3(1.21)	-0.36
Pd@G-O-OH-1b	NO	N	2.32	1.83	1.17	0.05
Pd@G-O-OH-1b	NO	O	0.96	1.98	1.17	0.01
Pd_6@G-2O-1a	NO	N at **2**	1.84	1.86	1.17	0.04
Pd_6@G-2O-1a	NO	N at **4**	2.06	1.84	1.17	0.04
Pd_6@G-2O-1a	NO	N at **5**	2.05	1.85	1.17	0.037
Pd_6@G-2O-1a	NO	N at **a**	1.74	2.13 (1.99)	1.19	-0.04
Pd_6@G-2O-1a	NO	N at **b**	2.0	2.02 (1.99)	1.2	-0.07

* The corresponding structures are shown Figures 8 and 11.

Table 5: The d-band center ε_d (in eV) and excess charge ΔQ (in *e*) over the isolated Pd cluster and rGO for atoms labeled in Figure 11.

Property	Pd**1**	Pd**2**	Pd**3**	Pd**4**	Pd**5**	Pd**6**	Pd/Pd_6*	O**1**	O**2**
ε_d	-2.23	-1.55	-1.83	-1.23	1.83	-1.53	-1.37		
ΔQ	-0.28	0.01	-0.08	-0.02	-0.08	0.0		0.12	0.12

* All atoms of isolated P_6 cluster have the same ε_d due to the symmetry of structure.

Figure captions

Figure 1. Geometrical structures of rGO with different atomic arrangement of hydroxyl and epoxide groups. (a) G-2O-1, (b) G-2O-2, (c) G-2OH-1, (d) G-2OH-2, (e) G-O-OH-1, (f) G-O-OH-2, (g) G-2O-OH-1, and (h) G-2O-OH-2. The number in (c) denotes the site of carbon atom.

Figure 2. Top and side views of optimized structure (distance in Å) of Pd adsorbed on graphene (a) and on rGO with one (b-c) and two (d-h) epoxide groups. (a) Pd@G, (b) Pd@G-O-a, (c) Pd@G-O-b, and (d)-(h) Pd@G-2O-1**i** with **i** = a, b, c, d, and e, respectively. The number in (f) and (g) marks the site of carbon atom.

Figure 3. Top and side views of optimized structure (distance in Å) of Pd adsorbed on rGO with two epoxide groups located at the opposite side each other (a-b) and with two hydroxyl groups (c-h). (a) Pd@G-2O-2a, (b) Pd@G-2O-2b, (c)-(g) Pd@G-2OH-1**i** with **i** = a, b, c, d, and e, respectively, and (h) Pd@G-2OH-2.

Figure 4. Top and side views of optimized structure (distance in Å) of Pd adsorbed on GOs with both epoxide and hydroxyl functional groups. (a) Pd@G-O-OH-1a, (b) Pd@G-O-OH-1b, (c)-(e) Pd@G-O-OH-2**i** and (f)-(h) Pd@G-2O-OH-1**i** with **i** = a, b, and c, respectively, (i) Pd@G-2O-OH-1d, and (j) Pd@G-2O-OH-2.

Figure 5. Top and side views of optimized structure (distance in Å) of Pd adsorbed on GOs containing sp^2 carbon regions separated by sp^3 carbon strips with high oxidation level. (a)-(c) Pd@GO-1**i** and (d)-(f) Pd@GO-2**i** with **i** = a, b, and, c, respectively.

Figure 6. The spin-polarized total density of states (TDOS) of GO with and without the Pd insertion. (a) G-2O-1 (the structure shown in Figure 1a), (b) Pd@G-2O-1a (Figure 2d), (c) Pd@G-2O-1c (Figure 2f), (d) Pd@G-2O-1e (Figure 2h), (e) G-2OH-2 (Figure 1d), (f) Pd@G-2OH-2 (Figure 3h), (g) G-2O-2 (Figure 1b), (h) Pd@G-2O-2b (Figure 3b), and (i) Pd@G-2OH-1b (Figure 3d). The Fermi level is set to 0.

Figure 7. Top and side views of optimized structure (distance in Å) of NO_2 adsorbed on Pd-decorated rGO with O or N-down adsorption orientation. (a)-(c) Pd@G-2O-1c, (d)-(e) Pd@G-2O-1d, (f) Pd@G-2O-1e, (g)-(h) Pd@G-2OH-2, and (i)-(j) Pd@G-O-OH-1b.

Figure 8. Top and side views of optimized structure (distance in Å) of NO_3 and NO adsorbed on Pd-decorated rGO. (a)-(c) Pd@G-2O-1c and (d)-(f) Pd@G-O-OH-1b.

Figure 9. The spin-polarized TDOS and PDOS for free (a) NO_2, (b) NO_3, and (c) the Pd and its binding site O for Pd@G-O-OH-1b. The TDOS (d, f) and PDOS (e, g) of Pd, NO_2, and adsorbed sites N or O atoms for NO_2 adsorbed on Pd@G-2O-1**c** with N-down (d)-(e) and O-down (f)-(g) adsorption orientations. The (h)-(j) for NO_2 adsorbed on Pd@G-O-OH-1b are similar with (d), (e), and (g), respectively. The TDOS (k) and PDOS (l) of Pd, NO_3, and binding site O atom of Pd for NO_3 adsorbed on Pd@G-2O-1**c**. The Fermi level is set to 0.

Figure 10. (a)-(c) and (i) The spin densities and (d)-(h) charge density difference for Pd atom and Pd cluster deposited rGO with and without NO_2 and NO_3 adsorption**. (a)-(f)** NO_2 and NO_3 adsorbed on Pd@G-2O-1**c**, (g) and (i) Pd_6@ G-2O-1-a, and (h) Pd_6@ G-2O-1-b. The blue and yellow areas in (a)-(c) and (i) with isosurfaces of 0.02 $e/Å^3$ denote the spin up and spin down, while these areas in (d)-(h) with isosurfaces of 0.05 $e/Å^3$ present electron accumulation and depletion, respectively.

Figure 11. Top and side views of optimized structure (distance in Å) for Pd_4 and Pd_6 deposited on G-2O-1 (a)-(d) and NO adsorbed on Pd_6-rGO hybrid (e)-(h). (a) Pd_4@ G-2O-1-a and (b) Pd_4@ G-2O-1-b, and (c) Pd_6@ G-2O-1-a and (d) Pd_6@ G-2O-1-b. The Pd and O atom sites and bridge sites are indicated in (c) and (d). Adsorption of NO at (e) Pd**2**, (f) Pd**4**, (g) **a**, and (h) **b** sites of Pd_6@ G-2O-1-a.

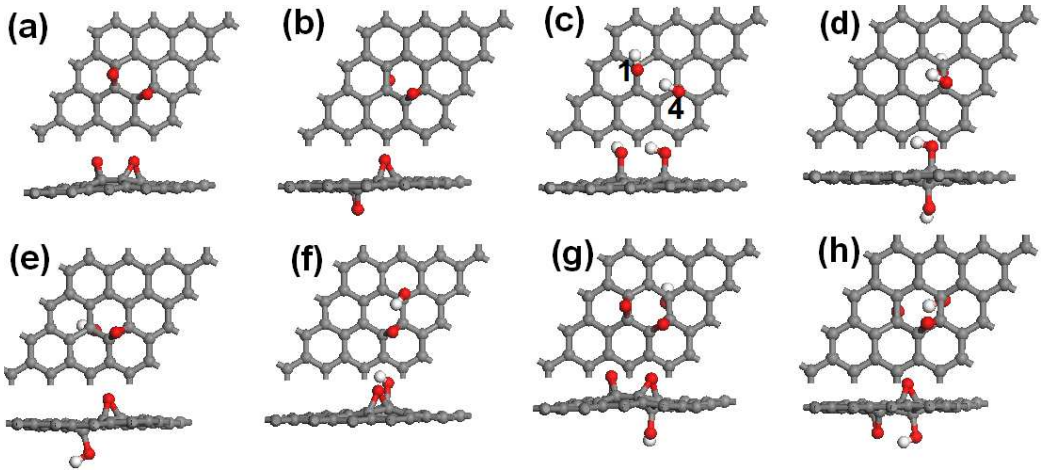

Figure 1.

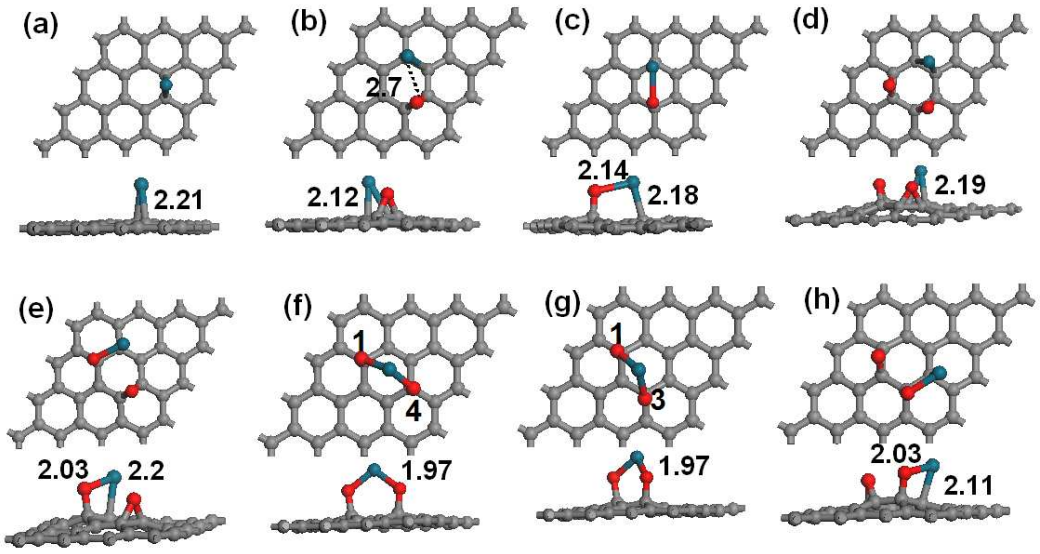

Figure 2.

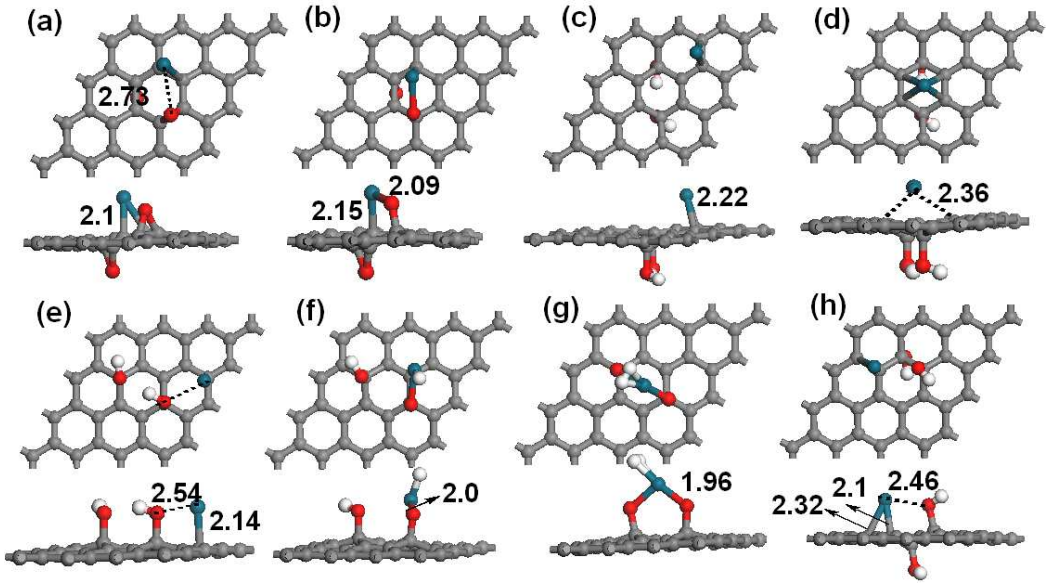

Figure 3.

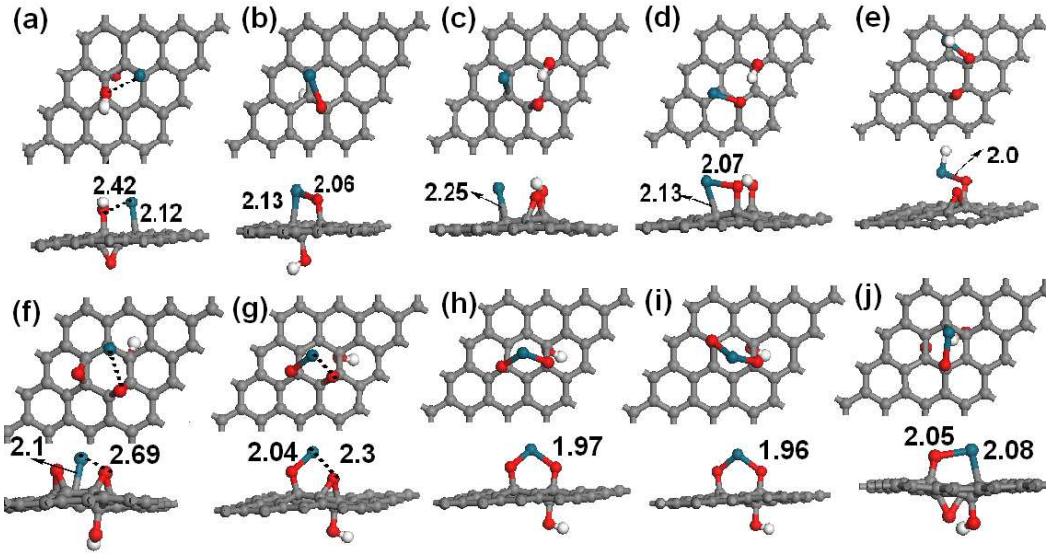

Figure 4.

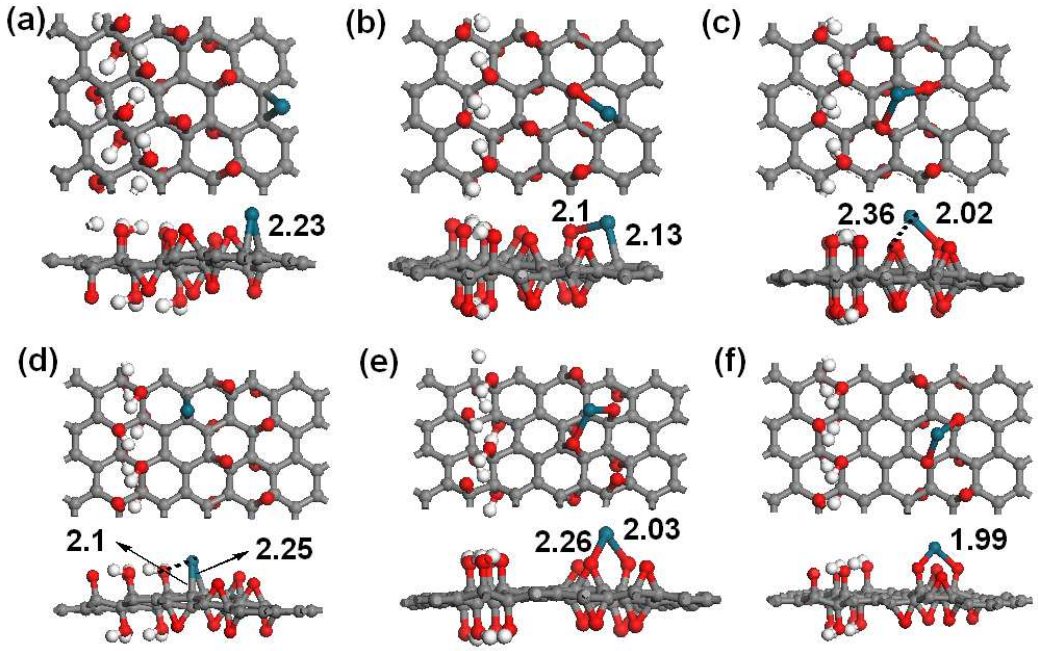

Figure 5.

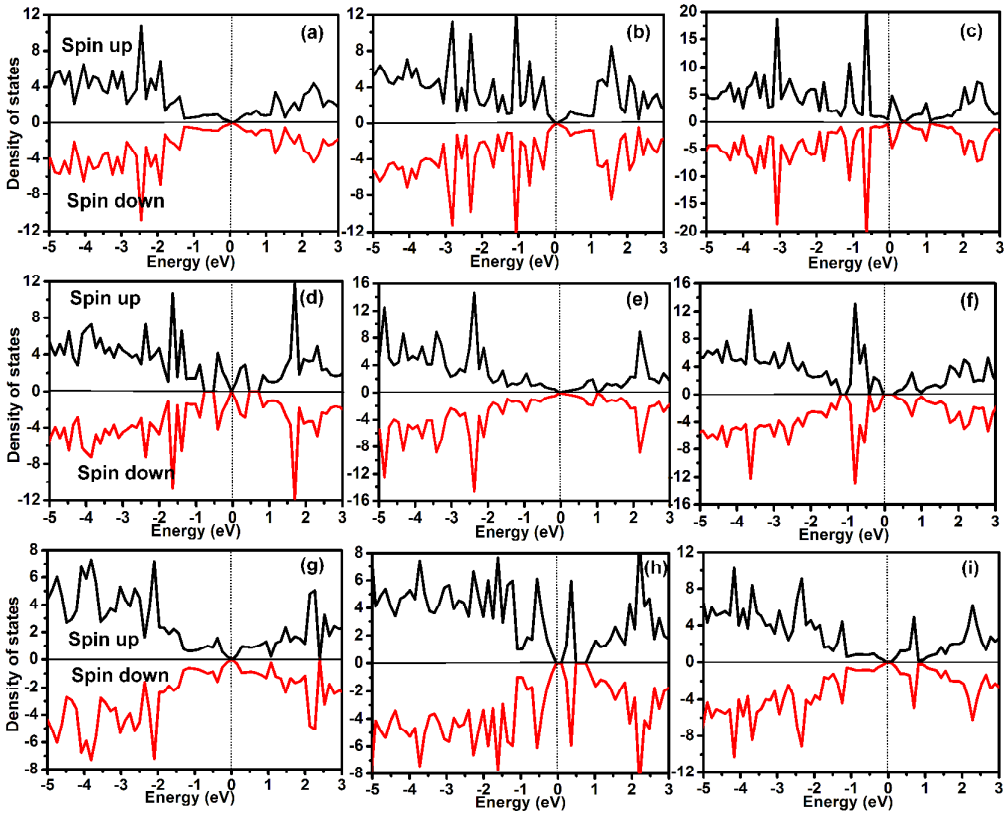

Figure 6.

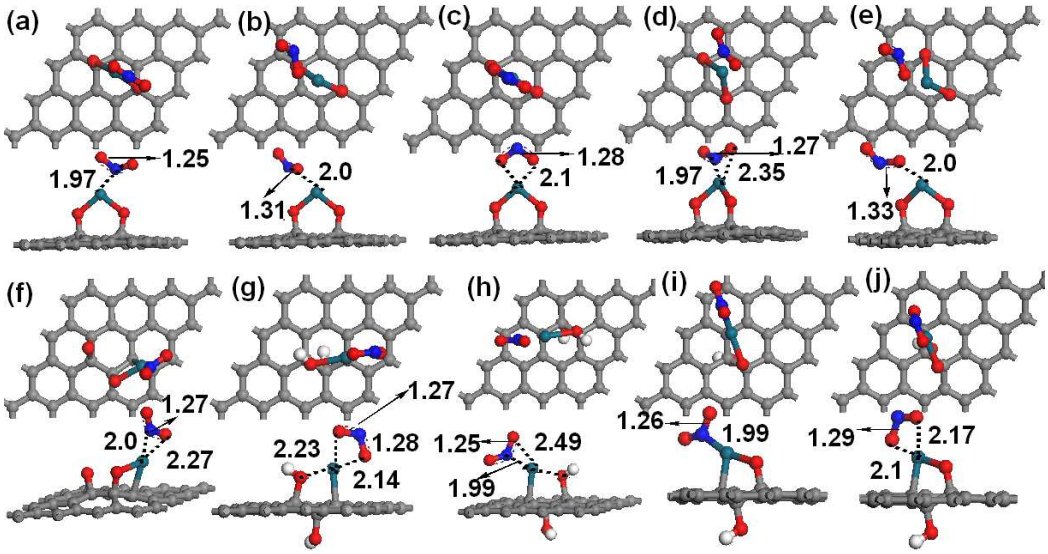

Figure 7

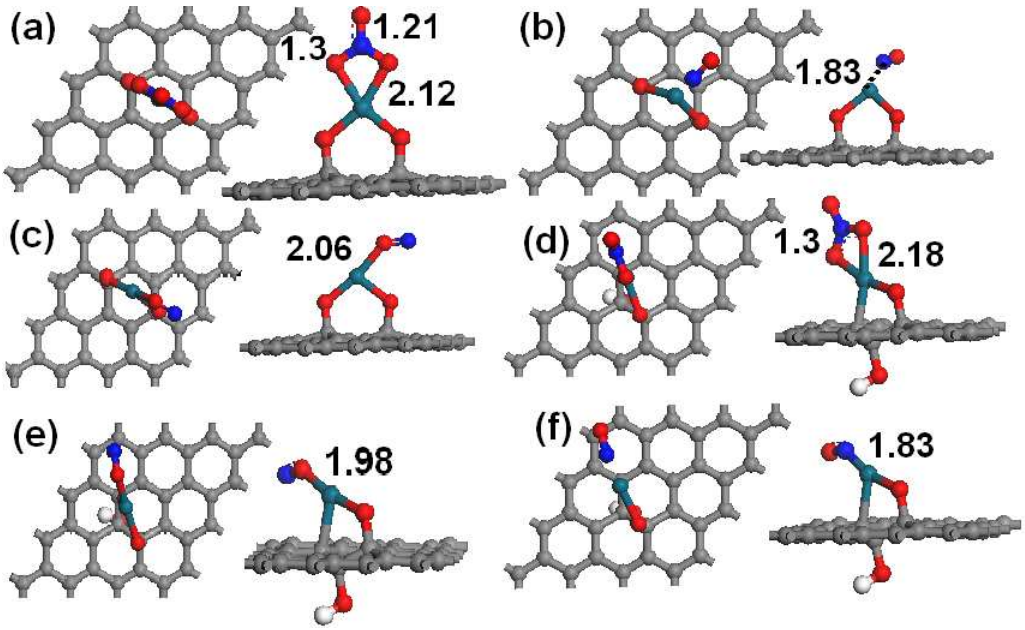

Figure 8

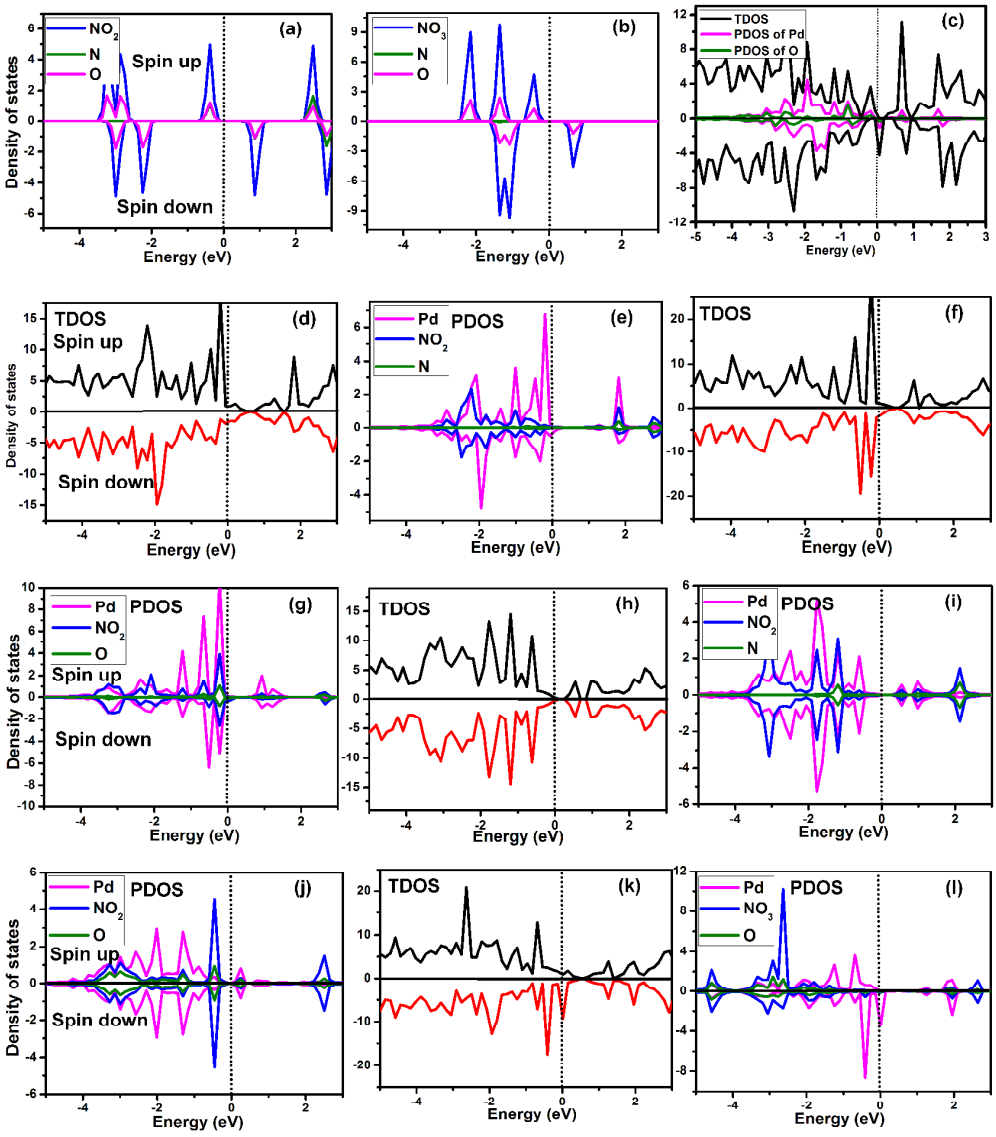

Figure 9

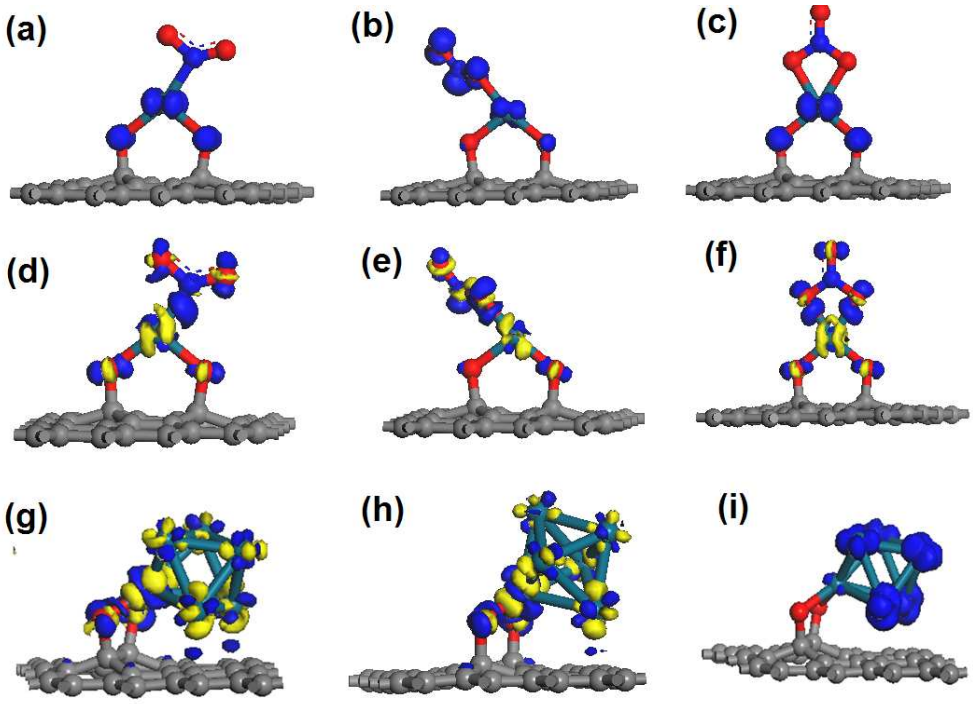

Figure 10

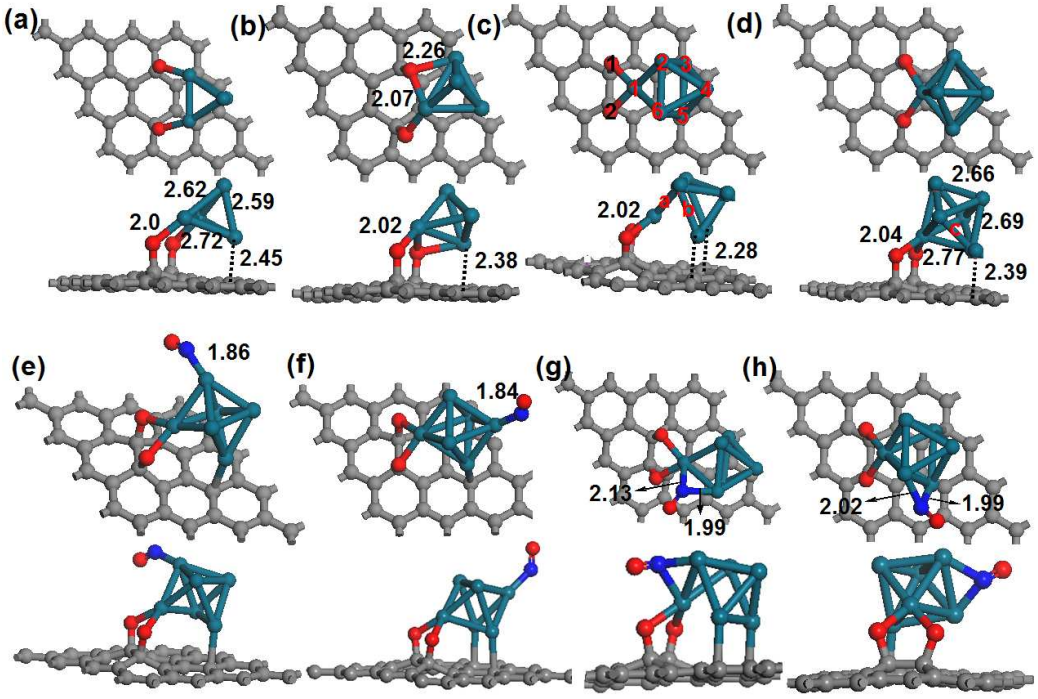

Figure 11.